Inorganic Chemistry

ARTICLE

pubs.acs.org/IC

Nanocrystals of $CeVO_4$ Doped by Metallic Heteroions

Yeqian Shen, Yucheng Huang, Sujuan Zheng, Xuefeng Guo, Zhao-Xu Chen,* Luming Peng,* and Weiping Ding

Key Laboratory of Mesoscopic Chemistry, School of Chemistry and Chemical Engineering, Nanjing University, Nanjing 210093, China

ABSTRACT: $CeVO_4$ nanocrystals doped by heteroions were prepared via a hydrothermal method without the presence of surfactants or templates. Transmission electron microscopy (TEM), high-resolution transmission electron microscopy (HRTEM), X-ray diffraction (XRD), solid state ^{51}V NMR, and inductively coupled plasma (ICP) were used to characterize the morphology, structure, and compositions of the materials. X-ray photoelectron spectroscopy (XPS) results confirmed that there is a valence change from Ce^{3+} to Ce^{4+} for a fraction of cerium atoms whereas the vanadium atoms remain in the pentavalent state V^{5+} upon the substitution of Ca^{2+} into $CeVO_4$. Raman spectroscopy was used to monitor the effects of the doping ion on the $CeVO_4$ lattice contraction and distortion. The appearance of the shifted and broadened Raman peaks for the doped $CeVO_4$ was interpreted by theoretical calculations performed with Vienna ab initio simulation package. The redox properties and photocatalytic activities of the obtained nanocrystals were also investigated and discussed in detail.

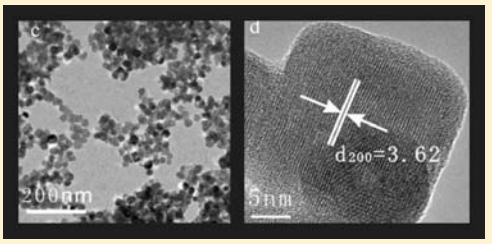

INTRODUCTION

Recently, inorganic nanoparticles with uniform size and shape have attracted a lot of research attention, since they are interesting from both theoretical and practical perspectives.[1,2] They possesses novel intrinsic properties in a wide variety of fields and have great potential as building blocks for bottom-up approaches to the fabrication of nanodevices.[3,4] Because dopants can be used to tune the electronic, optical, magnetic, and catalytic properties of the materials, over the past decade, intense research has been focused on doped nanomaterials, such as semiconductor nanocrystals (NCs),[5−7] photoluminescence NCs,[8−10] and nanocatalysts.[11] The intentional uniform introduction of impurities into a bulk material can usually be easily achieved; however, controllable doping without changing the size and shape of nanostructures is still a challenge because the impurity solubility is much lower in NCs than in the bulk materials, leading to the "self-purification" of the NCs,[12−14] which is not well understood yet.[15]

In recent years, much attention has been devoted to the study of rare earth orthovanadates ($LnVO_4$, Ln denotes a rare earth element), which form an important family of inorganic materials with wide application potential in various fields, such as catalysts,[16,17] polarizers,[18] laser host materials[19,20] and phosphors.[21−23] One of the most interesting and widely studied materials in the family is cerium(III) orthovanadate, $CeVO_4$. For example, for the catalytic oxidative dehydrogenation of propane, the tetragonal phase of $CeVO_4$ was found to be more active than the monoclinic phase of $LaVO_4$.[11] The naturally occurring $CeVO_4$ mineral, wakefieldite, crystallizes in a zircon-type ($I4_1/amd$) structure which consists of VO_4 tetrahedra sharing corners and edges with CeO_8 dodecahedra.[24] This tetragonal zircon-type structure stabilizes Ce^{3+} ion even under oxidizing conditions.[25] Since Ce^{3+}/Ce^{4+} and V^{5+}/V^{4+} redox states can be accessed in $CeVO_4$ by cation substitution, it provides methods to tune its redox property and rational design the materials for the use in electron transfer and catalysis. The structure, conductivity, redox properties,[26−30] as well as the photocatalytic properties,[11,31,32] have been explored to in undoped and doped $CeVO_4$ materials.

Therefore, the investigation on the doping effects on the $CeVO_4$ NCs should be interesting and important for exploring the novel physical and chemical properties of $CeVO_4$. Most previous approaches to the preparation of $CeVO_4$ NCs require organic templates and harsh reaction conditions,[32−36] or ultrasound/microwave is introduced to assist the synthesis.[31,37−39] Here, we present a facile and low-cost approach to synthesize pure and Ca^{2+} doped $CeVO_4$ NCs without organic template under hydrothermal conditions. Transmission electron microscopy (TEM), X-ray diffraction (XRD), X-ray photoelectron spectroscopy (XPS), ^{51}V solid-state NMR and Raman spectroscopy were used to characterize the NCs and investigate the doping effects. The theoretical calculation results for the frequencies of Raman modes of the $CeVO_4$ NCs were consistent with the experimental Raman data. Furthermore, the redox and photocatalytic properties of the undoped and doped $CeVO_4$ NCs were tested. The present study provides a rationale for the modified redox properties of $CeVO_4$:Ca (Ca^{2+} doped $CeVO_4$) NCs compared to that of $CeVO_4$ NCs. Extensions of this approach to prepare other rare earth orthovanadate NCs and study the doping effects can be readily envisaged.

EXPERIMENTAL SECTION

Preparations of the Nanocrystals (NCs). The $CeVO_4$ NCs were prepared by a simple hydrothermal method. In a typical preparation

Received: March 7, 2011
Published: May 31, 2011

procedure, 2.5 mmol of $Ce(NO_3)_3 \cdot 6H_2O$ and NH_4VO_3 were dissolved in 10 mL of 1 M HNO_3 and 10 mL of 1 M NaOH solvent, respectively. After 15 min stirring, the NH_4VO_3 solution was dropped into the $Ce(NO_3)_3$ solution, resulting in a bright yellow solution. The pH value was then adjusted to about 6 by 2 M NaOH solution, with the formation of a brown precipitate during the procedure. The mixture was magnetically stirred for about 4 h, and then transferred into a Teflon-lined autoclave with a stainless shell. The hydrothermal treatment proceeded at 180 °C for 24 h. The obtained brown precipitate was washed several times with distilled water and ethanol and finally dried under vacuum at 60 °C for 6 h. $CeVO_4$:Ca NCs were synthesized with a similar procedure as above: $Ce(NO_3)_3 \cdot 6H_2O$ and $CaCl_2$ were used as reactants in a mole ratio of 4:1 and 1:1, and 0.25 mL of 8.5% $N_2H_4 \cdot 6H_2O$ was added into the mixture as reducing agent after adjusting the pH value.

Characterizations of the NCs. TEM and HRTEM images were obtained on a JEOL JEM-2100 microscope. X-ray powder diffraction patterns were recorded on a Philips X'Perts X-ray powder diffractometer with Cu Kα radiation. The lattice parameters were determined by the X-ray powder diffraction with Si powders blended as inner standard. The amounts of Ca^{2+} in the doped samples were measured by ICP. The X-ray photoelectron spectra (XPS) measurements were made on an ESCALB MK-II spectrometer by using Mg Kα radiation as the excitation source. Binding energies were calibrated with respect to C_{1s} at 285.0 eV.[11] The Raman spectra were obtained on a Renishaw spectrometer equipped with a CCD detector at ambient temperature condition. The emission line at 514 nm from an Ar ion laser was focused. The power of incident bean on the sample was ~20 mW. Room temperature ^{51}V MAS NMR experiments were performed with a 4.0 mm MAS probe on a Bruker Avance III spectrometer in a magnetic field strength of 9.4 T at a Larmor frequency of 105.181 MHz. Powdered samples were packed inside zirconia MAS rotors and spun at 14 kHz. The ^{51}V MAS spectra were obtained using a single hard pulse, with the radiofrequency (rf) power of 83 kHz. To obtain more quantitative spectra, a $\pi/8$ pulse duration was employed, resulting in 0.2 μs long pulses for the single-pulse experiments. Recycle delays of 0.2 s were used for ^{51}V MAS experiments. ^{51}V chemical shifts were referenced to the external standard, $VOCl_3$, which was set at 0.0 ppm.[40]

Theoretical Calculations. The calculations for the vibrational modes of the NCs were performed with the plane-wave based Vienna ab initio simulation package (VASP)[41] using the generalized-gradient approximation PW91 as exchange-correlation functional.[42−45] The interaction between atomic cores and electrons was described by the projector augmentation wave (PAW) method.[43,46] Brillouin-zone integrations were done with Monkhorst−Pack grids[47] using a generalized Gaussian smearing[48] width of 0.1 eV. A (12 × 12 × 12) k-point grid was selected for lattice constant optimization of $CeVO_4$ crystal, while only γ-point for the calculation of vibration frequency of $CeVO_4$ nanocrystal .

Temperature-Programmed Reduction (TPR). The hydrogen TPR experiments were carried out on a homemade analyzer with thermal conduction detector (TCD). In a typical experiment, 30 mg of the sample was placed in a U type quartz tube and heated in a heliumflow at 673 K for 1 h. The flowing gas was switched to H_2/Ar (10%, 30 cm^3/min) when the sample was cooled to room temperature. After that, the sample was heated at 10 K/min for the TPR experiment. A thermal conductivity detector (TCD) was used to record the signal of H_2 consumption.

Photochemical Reaction. An LS-SXE300 Xenon lamp was used for the degradation reactions. The solution with desired methylene blue concentration was stirred with the NCs in the dark before the light was turned on for the photocatalytic reaction. After certain period of time, the samples were centrifuged before analysis. Photometric studies were carried out for the dye used. The UV−vis spectrophotometer (Shimadzu, UV-300) with quartz cuvettes was used to determine the color intensity in the range of 190−700 nm.

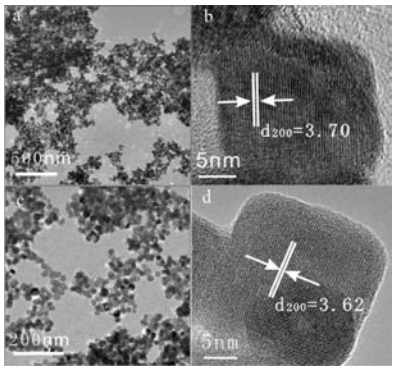

Figure 1. (a) and (b) TEM and HRTEM images of the $CeVO_4$ NCs synthesized by hydrothermal method; (c) and (d) TEM and HRTEM images of the $CeVO_4$:Ca (6.29%) NCs.

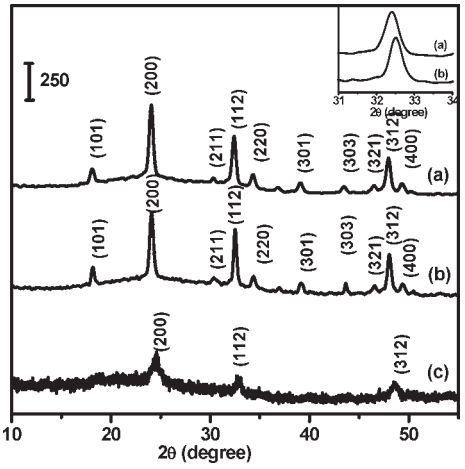

Figure 2. XRD patterns of NCs: (a) $CeVO_4$; (b) $CeVO_4$:Ca (6.29%) and (c) $CeVO_4$:Ca (46.2%); inset is the enlarged patterns of reflection peak at around 2θ = 32.6° of (a) $CeVO_4$, (b) $CeVO_4$:Ca (6.29%).

RESULTS AND DISCUSSION

Tetragonal $CeVO_4$ NCs can be obtained by using $Ce(NO_3)_3 \cdot 6H_2O$ and NH_4VO_3 as starting materials through hydrothermal treatment without any template. A typical TEM image of $CeVO_4$ NCs is shown in Figure 1a. The as-synthesized $CeVO_4$ NCs exhibit a cube-like morphology with a width of 10−20 nm. The HRTEM image shows that the NCs are structurally uniform with an interplanar spacing of about 3.70 Å which corresponds to the (200) lattice spacing of $CeVO_4$ (Figure 1b). The clear lattice fringes in the HRTEM images confirm the high crystallinity of the NCs. TEM and HRTEM images of Ca^{2+} doped $CeVO_4$ NCs, which also possess a cube-like morphology, are shown in Figure 1c and 1d, respectively. The interplanar spacing that corresponds to the (200) lattice spacing of $CeVO_4$, however, is reduced to about 3.62 Å.

The ICP results show the mole percentages of Ca^{2+} are 6.29% and 46.2%, for the samples synthesized with 4:1 and 1:1 Ce:Ca ratios of the reactants, respectively. It appears that the Ca^{2+} contents in the doped $CeVO_4$ NCs, especially $CeVO_4$:Ca (6.29%) NCs, are significantly less than that in the initial compositions, which is consistent with the "self-purification" mechanism of the NCs.[12−14] The Ca concentration in the $CeVO_4$:Ca (46.2%) NCs is slightly higher than the upper limit

(41.25%) for the bulk $Ce_{1-x}Ca_xVO_4$ solid-solution, where a second phase $Ca_2V_2O_7$ starts to form according to the results by Petit and co-workers.[28]

The XRD patterns shown in Figure 2 further verify the chemical compositions and structures of the $CeVO_4$ and the Ca-doped $CeVO_4$ NCs. All of the reflection peaks of the $CeVO_4$ NCs in the Figure 2a can be indexed to the tetragonal structured $CeVO_4$, while they show small displacements in the Ca-doped NCs (Figure 2b and 2c). The enlarged region of the (112) reflection peak for the Ca-doped NCs is associated with a smaller *d*-spacing (inset of Figure 2), indicating a decrease in lattice parameters after doping. The refined cell parameters of the $CeVO_4$ and $CeVO_4$:Ca (6.29%) NCs confirms lattice contraction (Table 1). This phenomenon has also been observed in the bulk Ca^{2+} doped $CeVO_4$ materials. The ionic radius of 8-coordinated Ca^{2+} (1.12 Å) is only slightly smaller than Ce^{3+} (1.143 Å); therefore, the lattice contraction is not likely due to Ce^{3+} being partially replaced by Ca^{2+}. It can be explained through the formation of the much smaller Ce^{4+} (0.97 Å) to balance the charge upon Ca^{2+} doping.[28,30] Previous results for the bulk Ca-doped $CeVO_4$ materials show a trend in which the contraction is more significant in the *a*- or *b*-axis than in the *c*-axis.[27,28,30] In our results, however, the contraction is found to be more in the *c*-axis (13.5%) than in the *a* or *b* axis (11.9%) (Figure 3), presumably because of the surface effect of the NCs.

Table 1. Crystal Cell Parameters of the NCs of the Pure and Doped $CeVO_4$

samples	$CeVO_4$	$CeVO_4$:Ca (6.29%)
$a = b$	7.407(1)	7.318(1)
c	6.540(1)	6.451(1)
$\alpha = \beta = \gamma$	90	90

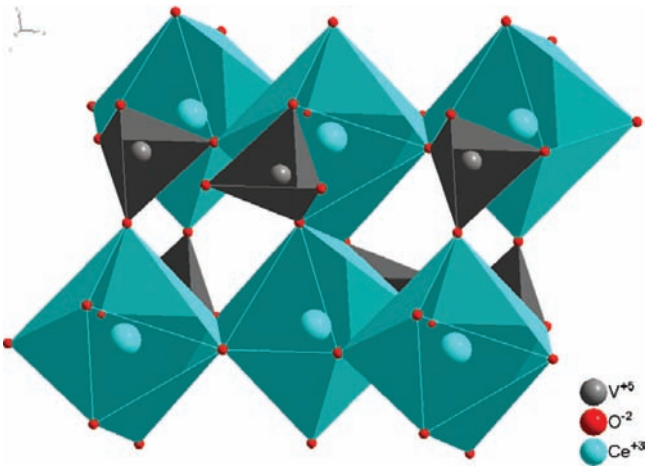

Figure 3. Crystal structure of the zircon-type $CeVO_4$ with VO_4 tetrahedra and CeO_8 dodecahedra.

Since Ce^{3+}/Ce^{4+} and V^{5+}/V^{4+} are the two pairs of redox states that can be accessed in $CeVO_4$, XPS was used to investigate the effects on the electronic structure change of both Ce and V ions after Ca^{2+} doping, in particular, whether Ce^{4+} is formed upon Ca^{2+} doping. Figure 4a shows the core level spectra of Ce $3d_{5/2}$ and Ce $3d_{3/2}$ of $CeVO_4$ NCs with the binding energies of Ce 3d and V 2p photoelectron peaks presented in Table 2. The peaks at 881.65 and 885.4 eV correspond to the Ce $3d_{5/2}$ transitions, while the peaks at 900.41 and 903.99 eV belong to the Ce $3d_{3/2}$ binding energy. The binding energies at 885.4 and 903.99 eV represent the $3d^{10}4f^1$ initial electronic state corresponding to Ce^{3+} and no peak associated with Ce^{4+} was found, which is consistent with previous results of $CeVO_4$ nanocrystals[36,39] and bulk materials.[49] The Ce 3d XPS profile of $CeVO_4$:Ca (6.29%) NCs (Figure 4b) shows a small new peak at about 917.4 eV, which is the fingerprint of Ce^{4+} species, indicating that a fraction of Ce^{3+} ions was oxidized for the charge

Table 2. XPS Binding Energy (eV) of $CeVO_4$ and $CeVO_4$:Ca (6.29%) NCs

	CeO_2[43]	$CePO_4$[44]	$CeVO_4$[45]	$CeVO_4$	$CeVO_4$:Ca
V $2p_{3/2}$			517.45	517.3	517.4
V $2p_{1/2}$			524.72	524.9	525.3
Ce $3d_{5/2}$(I)	882.4	885.4	882.41	881.6	881.6
Ce $3d_{5/2}$(II)			886.41	885.4	885.7
Ce $3d_{3/2}$(I)		904	901.15	900.4	899.6
Ce $3d_{3/2}$(II)			905.13	904.0	904.7
Ce $3d_{3/2}$(III)	916.7				917.4

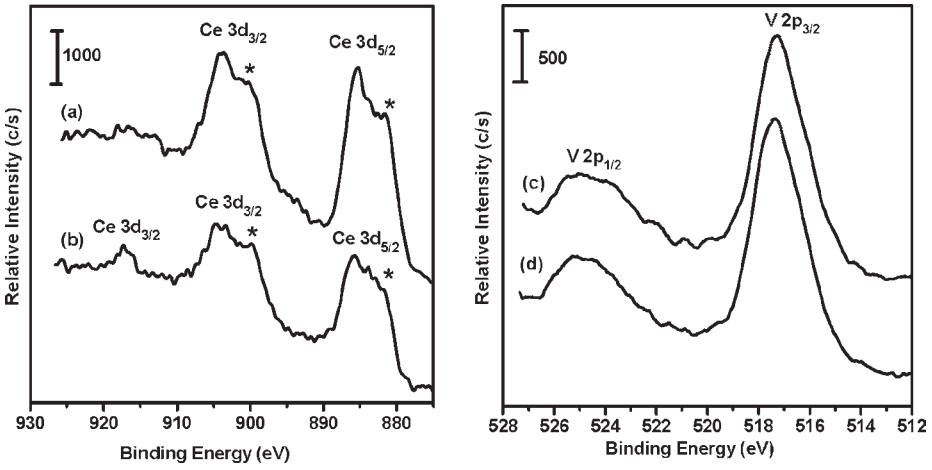

Figure 4. Ce 3d XPS spectra of (a) $CeVO_4$; (b) $CeVO_4$:Ca (6.29%) NCs, * denotes Ce^{3+} satellite peak; V 2p XPS spectra of (c) $CeVO_4$; (d) $CeVO_4$:Ca NCs.

dx.doi.org/10.1021/ic200459t |*Inorg. Chem.* 2011, 50, 6189–6194

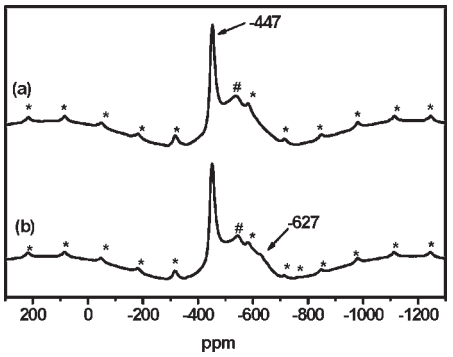

Figure 5. ^{51}V MAS NMR spectra of (a) $CeVO_4$ NCs and (b) $CeVO_4$:Ca (6.29%) NCs. * denotes spinning sidebands; # denotes a broad signal tentatively assigned to impurities.

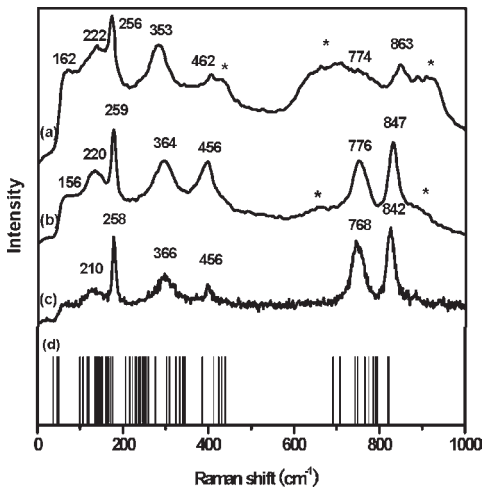

Figure 6. Raman spectra of (a) $CeVO_4$:Ca (46.2%) NCs; (b) $CeVO_4$:Ca (6.29%) NCs; (c) $CeVO_4$ NCs. (d) Theoretically calculated frequencies of $CeVO_4$. *: VO_4 vibration influenced by doping Ca^{2+}.

compensation. The presence of Ce^{4+} is consistent with the lattice contraction observed. On the other hand, the binding energies of V $2p_{3/2}$ and V $2p_{1/2}$ are very similar in both $CeVO_4$ and $CeVO_4$:Ca NCs (Table 2), thus vanadium is still in +5 state in doped $CeVO_4$.

^{51}V is a spin-7/2 quadrupolar nucleus with 100% natural abundance and a fairly high gyromagnetic ratio. Solid-state ^{51}V NMR spectroscopy represents a sensitive method to probe the local structure of V^{5+} ions in many technologically important materials, such as V_2O_5-containing catalysts.[50] Recently rich information has also been extracted from vanadia nanoparticles;[51] therefore, ^{51}V MAS NMR spectroscopy (Figure 5) was used to investigate the influence of calcium insertion on the environment of the anions in the $CeVO_4$ NCs (Figure 4). A single sharp resonance can be observed at −447 ppm with spinning sidebands for undoped NCs, which corresponds to VO_4 species associated with Ce only.[52,53] For the Ca-doped sample, in addition to the major signal at −447 ppm, a weak resonance shows up at −627 ppm, which can be assigned to the VO_4 with Ca^{2+} nearby,[54] indicating the Ca^{2+} ions are introduced into the lattice. The large difference of 180 ppm (18.9 kHz at 9.4 T) in the resonant frequencies between the two species demonstrates the significant changes in the electronic environment of vanadium introduced by Ca^{2+} and subsequent formation of Ce^{4+}. Therefore, the Ca^{2+} doping should have a large impact on the redox property and catalytic activity of $CeVO_4$. In principle, the spinning sideband manifolds can also provide useful information about the distortion at the V site;[52,55] however, only one set of spinning sideband can be observed for the peak of VO_4 associated with Ca^{2+} presumably because of the small concentration of the species and/or the significant chemical shift distribution.

Table 3. Theoretical Calculations of Raman Spectrum of $CeVO_4$

Raman frequency (exp.) /cm^{-1}	Raman frequency (cal.)/cm^{-1}	assignment
842	794.8	A_{1g} VO_4^{3-} symmetric stretch (ν_1)
768	775.6	E_g VO_4^{3-} asymmetric stretch (ν_3)
	765.9	
	708.4	
	707.4	
	691.7	
456	439.6	$E_g + B_{2g}$ VO_4^{3-} deformation (ν_4)
	431.2	
366	341.6	$A_{1g} + B_{1g}$ VO_4^{3-} deformation (ν_2)
	339.3	
258	206.8	CeO_8 stretch
166	176.8	B_{1g} O−Ce−O deformation
	151.8	

The nanocrystals were further studied by experimental as well as theoretical calculations of Raman spectra. Theoretical Raman calculation results are depicted in Figure 6d. The vertical lines are the 72 calculated vibration modes of $CeVO_4$ crystals; however, only 24 modes are active for Raman scattering. The calculation results matched well with the experimental Raman spectra (Table 3) considering the error associated with the calculation model. In the Raman spectrum of $CeVO_4$ (Figure 6c), four main Raman modes are observed at 366, 456, 768, and 842 cm^{-1}, which arise from $A_{1g} + B_{1g}$ deformation (ν_2), $E_g + B_{2g}$ deformation (ν_4), E_g asymmetric stretch (ν_3), and A_{1g} symmetric stretch (ν_1) of VO_4^{3-}, respectively,[56−59] while the 259 cm^{-1} mode can be assigned to CeO_8 stretch, according to the theoretical calculation results. On substitution of the aliovalent cations Ca^{2+} (Figure 6b), broad Raman bands emerge at approximately 492, 694, 903 cm^{-1} (denoted * in Figure 6b) and the intensities of these bands increase with increasing Ca^{2+} dopant (Figure 6a). The A_{1g} symmetric stretch mode at 842 cm^{-1} shifts upward, whereas the $A_{1g} + B_{1g}$ deformation mode at 366 cm^{-1} shifts downward with increasing Ca^{2+} amount. On the basis of the Raman investigations, a reasonable explanation for the appearance of three broad bands in Ca doped $CeVO_4$ can be described as follows. When Ca^{2+} is substituted for Ce^{3+} in $CeVO_4$ NCs, a fraction of Ce^{3+} is oxidized to Ce^{4+} for charge compensation. The smaller ionic radius of Ce^{4+} also causes lattice contraction. The oxygen content may remain stoichiometric or with oxygen excess, according to the conductivity measurement results.[27] The scenario of oxygen deficiency in doped $CeVO_4$ NCs, however, cannot be completely ruled out in case less Ce^{4+} is present for charge compensation. Nonetheless, the above factors affect the local environment around the pentavalent V atoms, resulting in shortened V−O bands and modified vibrational frequencies, which are associated with the

dx.doi.org/10.1021/ic200459t |*Inorg. Chem.* 2011, 50, 6189–6194

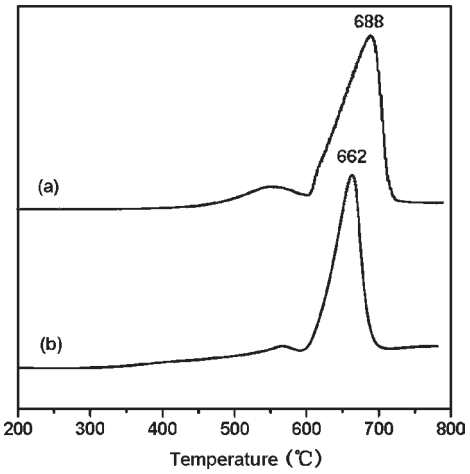

Figure 7. TPR profiles of (a) $CeVO_4$ NCs; (b) $CeVO_4$:Ca (6.29%) NCs.

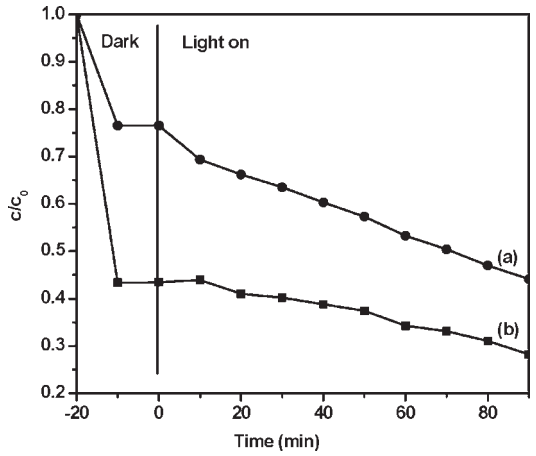

Figure 8. Photocatalytic degradation profile of methylene blue in the presence of (a) $CeVO_4$ NCs; (b) $CeVO_4$:Ca (6.29%) NCs.

appearance of the broadened bands. Meanwhile, the shortening of the V−O length, which causes an increase in force constants, changes the A_{1g} symmetric stretch mode from 842 cm^{-1} to 847 cm^{-1}, which is consistent with the results in the literature.[57] As for the $A_{1g} + B_{1g}$ deformation mode, the force constants decrease because of the distortion of VO_4 tetrahedra with the cation substitution, resulting in the downward shift of the mode.

The influences of calcium substitution on the redox property of $CeVO_4$ were investigated by H_2/TPR (Figure 7). The TPR profile of $CeVO_4$ exhibits a main peak at 688 °C along with a weaker peak at about 550 °C, which may arise from the reduction of bulk and surface vanadium ion V^{5+} to V^{4+}, respectively.[11] For the $CeVO_4$:Ca (6.29%) NCs, the main peak shifts to a lower temperature with the maximum at 662 °C, indicating that the lattice oxygen in Ca^{2+} ion-substituted $CeVO_4$ NCs is more active than that in $CeVO_4$ NCs. This again can be partially attributed to the structure distortion of $CeVO_4$:Ca because of the difference in ionic radii of the cations. Meanwhile, the charge transfer effects on the aliovalent cation substitution, which preserves charge neutrality via the oxidation of Ce^{3+} and possible change in chemical stoichiometry, should play an important role in controlling the redox property of $CeVO_4$.

The photocatalytic degradation of methylene blue was investigated in presence of $CeVO_4$ and $CeVO_4$:Ca (6.29%) NCs, and the profiles are shown in Figure 8. The solution with desired dye concentration was stirred with NCs in the dark, and it takes only about 10 min to achieve a balance between adsorption and desorption. Significant decrease in the concentration of dyes (56.5%) was observed for $CeVO_4$:Ca (6.29%) NCs, presumably because of the strong adsorption originated from surface defects associated with the doping. After 80 min of photocatalytic reaction, the concentration of the dye with $CeVO_4$ NCs and $CeVO_4$:Ca (6.29%) NCs decreased to 47% and 31%, respectively. Although the concentration of methylene blue in the presence of $CeVO_4$:Ca (6.29%) NCs decreased more than that with $CeVO_4$ NCs as the catalyst, the photodegradation performance is not better. Since the specific surface area of the pure and doped NCs is similar, the small difference in photocatalytic performance may be attributed to the slight difference in the acidity on the surface.

CONCLUSION

In summary, undoped and Ca^{2+} doped $CeVO_4$ NCs with a cube-like morphology were prepared via a facile approach without any organic templates. A wide variety of methods were used to investigate the structure and properties of the NCs. Compared to the bulk materials, $CeVO_4$ NCs showed a different lattice contraction behavior, while a higher Ca^{2+} doping level (up to 46.2%) was achieved in the NCs. A new signal showed up in ^{51}V MAS NMR for doped NCs, indicating that the Ca^{2+} ions were successfully introduced into the lattice. XPS data proved that a fraction of Ce was oxidized to Ce^{4+} while vanadium was still in +5 state in Ca^{2+} doped $CeVO_4$ NCs. Theoretical Raman results were consistent with the experimental data and the vibrational frequency change upon doping was associated with the shortened V−O bond length. The test on redox and photocatalytic properties of the undoped and doped $CeVO_4$ NCs showed that the lattice oxygen atoms were more active and the adsorption for methylene blue was also stronger in the doped nanomaterials.

AUTHOR INFORMATION

Corresponding Author

*E-mail: luming@nju.edu.cn (L.P.), zxchen@nju.edu.cn (Z.C.). Fax: +86-25-83317761. Phone: +86-25-83595077.

ACKNOWLEDGMENT

We are grateful to the financial support from the MOST of China (Grant 2009CB623504) and the NSF of China (Grant 20903056).

REFERENCES

(1) Alivisatos, A. P. *Science* **1996**, *271*, 933.
(2) El-Sayed, M. A. *Acc. Chem. Res.* **2001**, *34*, 257.
(3) Carbone, L.; Kudera, S.; Giannini, C.; Ciccarella, G.; Cingolani, R.; Cozzoli, P. D.; Manna, L. *J. Mater. Chem.* **2006**, *16*, 3952.
(4) Polleux, J.; Antonietti, M.; Niederberger, M. *J. Mater. Chem.* **2006**, *16*, 3969.
(5) Chen, D. A.; Viswanatha, R.; Ong, G. L.; Xie, R. G.; Balasubramaninan, M.; Peng, X. G. *J. Am. Chem. Soc.* **2009**, *131*, 9333.
(6) Hanif, K. M.; Meulenberg, R. W.; Strouse, G. F. *J. Am. Chem. Soc.* **2002**, *124*, 11495.

(7) Nag, A.; Chakraborty, S.; Sarma, D. D. *J. Am. Chem. Soc.* **2008**, *130*, 10605.
(8) Jia, C. J.; Sun, L. D.; Luo, F.; Jiang, X. C.; Wei, L. H.; Yan, C. H. *Appl. Phys. Lett.* **2004**, *84*, 5305.
(9) Lehmann, O.; Kompe, K.; Haase, M. *J. Am. Chem. Soc.* **2004**, *126*, 14935.
(10) Riwotzki, K.; Meyssamy, H.; Kornowski, A.; Haase, M. *J. Phys. Chem. B* **2000**, *104*, 2824.
(11) Bellakki, M. B.; Baidya, T.; Shivakumara, C.; Vasanthacharya, N. Y.; Hegde, M. S.; Madras, G. *Appl. Catal., B* **2008**, *84*, 474.
(12) Dalpian, G. M.; Chelikowsky, J. R. *Phys. Rev. Lett.* **2006**, *96*, 226802.
(13) Erwin, S. C.; Zu, L. J.; Haftel, M. I.; Efros, A. L.; Kennedy, T. A.; Norris, D. J. *Nature* **2005**, *436*, 91.
(14) Norris, D. J.; Efros, A. L.; Erwin, S. C. *Science* **2008**, *319*, 1776.
(15) Fa, W.; Dong, J. M. *J. Chem. Phys.* **2008**, 128.
(16) Fang, Z. M.; Hong, Q.; Zhou, Z. H.; Dai, S. J.; Weng, W. Z.; Wan, H. L. *Catal. Lett.* **1999**, *61*, 39.
(17) Martinez-Huerta, M. V.; Coronado, J. M.; Fernandez-Garcia, M.; Iglesias-Juez, A.; Deo, G.; Fierro, J. L. G.; Banares, M. A. *J. Catal.* **2004**, *225*, 240.
(18) Terada, Y.; Shimamura, K.; Kochurikhin, V. V.; Barashov, L. V.; Ivanov, M. A.; Fukuda, T. *J. Cryst. Growth* **1996**, *167*, 369.
(19) Fields, R. A.; Birnbaum, M.; Fincher, C. L. *Appl. Phys. Lett.* **1987**, *51*, 1885.
(20) Oconnor, J. R. *Appl. Phys. Lett.* **1966**, *9*, 407.
(21) Gambino, J. R.; Guare, C. J. *Nature* **1963**, *198*, 1084.
(22) Huignard, A.; Gacoin, T.; Boilot, J. P. *Chem. Mater.* **2000**, *12*, 1090.
(23) Stouwdam, J. W.; Raudsepp, M.; van Veggel, F. C. J. M. *Langmuir* **2005**, *21*, 7003.
(24) Chakoumakos, B. C.; Abraham, M. M.; Boatner, L. A. *J. Solid State Chem.* **1994**, *109*, 197.
(25) Watanabe, A. *J. Solid State Chem.* **2000**, *153*, 174.
(26) Tsipis, E. V.; Kharton, V. V.; Vyshatko, N. P.; Shaula, A. L.; Patrakeev, M. V.; Frade, J. R. *Ionics* **2003**, *9*, 231.
(27) Tsipis, E. V.; Patrakeev, M. V.; Kharton, V. V.; Vyshatko, N. P.; Frade, J. R. *J. Mater. Chem.* **2002**, *12*, 3738.
(28) Petit, C. T. G.; Lan, R.; Cowin, P. I.; Kraft, A.; Tao, S. W. *J. Mater. Sci.* **2011**, *46*, 316.
(29) Petit, C. T. G.; Lan, R.; Cowin, P. I.; Tao, S. W. *J. Solid State Chem.* **2010**, *183*, 1231.
(30) Tsipis, E. V.; Kharton, V. V.; Vyshatko, N. P.; Shaula, A. L.; Frade, J. R. *J. Solid State Chem.* **2003**, *176*, 47.
(31) Mahapatra, S.; Nayak, S. K.; Madras, G.; Row, T. N. G. *Ind. Eng. Chem. Res.* **2008**, *47*, 6509.
(32) Selvan, R. K.; Gedanken, A.; Anilkumar, P.; Manikandan, G.; Karunakaran, C. *J. Cluster Sci.* **2009**, *20*, 291.
(33) Liu, J. F.; Wang, L. L.; Sun, X. M.; Zhu, X. Q. *Angew. Chem., Int. Ed.* **2010**, *49*, 3492.
(34) Deng, H.; Yang, S. H.; Xiao, S.; Gong, H. M.; Wang, Q. Q. *J. Am. Chem. Soc.* **2008**, *130*, 2032.
(35) Liu, J. F.; Li, Y. D. *J. Mater. Chem.* **2007**, *17*, 1797.
(36) Nguyen, T. D.; Dinh, C. T.; Do, T. O. *Langmuir* **2009**, *25*, 11142.
(37) Yu, C. C.; Yu, M.; Li, C. X.; Zhang, C. M.; Yang, P. P.; Lin, J. *Cryst. Growth Des.* **2009**, *9*, 783.
(38) Wang, H.; Meng, Y. Q.; Yan, H. *Inorg. Chem. Commun.* **2004**, *7*, 553.
(39) Zhu, L.; Li, Q.; Li, J. Y.; Liu, X. D.; Meng, J.; Cao, X. Q. *J. Nanopart. Res.* **2007**, *9*, 261.
(40) Skibsted, J.; Nielsen, N. C.; Bildsoe, H.; Jakobsen, H. J. *Chem. Phys. Lett.* **1992**, *188*, 405.
(41) Kresse, G.; Hafner, J. *Phys. Rev. B* **1993**, *47*, 558.
(42) Perdew, J. P.; Chevary, J. A.; Vosko, S. H.; Jackson, K. A.; Pederson, M. R.; Singh, D. J.; Fiolhais, C. *Phys. Rev. B* **1992**, *46*, 6671.
(43) Blochl, P. E. *Phys. Rev. B* **1994**, *50*, 17953.
(44) Kresse, G.; Hafner, J. *Phys. Rev. B* **1994**, *49*, 14251.
(45) Perdew, J. P.; Wang, Y. *Phys. Rev. B* **1992**, *45*, 13244.
(46) Kresse, G.; Furthmuller, J. *Comput. Mater. Sci.* **1996**, *6*, 15.
(47) Monkhorst, H. J.; Pack, J. D. *Phys. Rev. B* **1976**, *13*, 5188.
(48) Methfessel, M.; Paxton, A. T. *Phys. Rev. B* **1989**, *40*, 3616.
(49) Salvi, A. M.; Decker, F.; Varsano, F.; Speranza, G. *Surf. Interface Anal.* **2001**, *31*, 255.
(50) MacKenzie, K. J. D.; Smith, M. E. *Multinuclear Solid-State NMR of Inorganic Materials*; Pergamon: Elmsford, NY, 2002; Vol. 6.
(51) Nielsen, U. G.; Topsoe, N. Y.; Brorson, M.; Skibsted, J.; Jakobsen, H. J. *J. Am. Chem. Soc.* **2004**, *126*, 4926.
(52) Cousin, R.; Courcot, D.; Abi-Aad, E.; Capelle, S.; Amoureux, J. P.; Dourdin, M.; Guelton, M.; Aboukais, A. *Colloid Surf., A* **1999**, *158*, 43.
(53) Radhika, T.; Sugunan, S. *J. Mol. Catal. A: Chem.* **2006**, *250*, 169.
(54) Pizzala, H.; Caldarelli, S.; Eon, J. G.; Rossi, A. M.; Laurencin, D.; Smith, M. E. *J. Am. Chem. Soc.* **2009**, *131*, 5145.
(55) Cousin, R.; Abi-Aad, E.; Capelle, S.; Courcot, D.; Lamonier, J. F.; Aboukais, A. *J. Mater. Sci.* **2007**, *42*, 6188.
(56) Baran, E. J.; Escobar, M. E.; Fournier, L. L.; Filgueira, R. R. *Z. Anorg. Allg. Chem.* **1981**, *472*, 193.
(57) Hirata, T.; Watanabe, A. *J. Solid State Chem.* **2001**, *158*, 254.
(58) Hirata, T.; Watanabe, A. *J. Solid State Chem.* **2001**, *158*, 264.
(59) Krasovec, U. O.; Orel, B.; Surca, A.; Bukovec, N.; Reisfeld, R. *Solid State Ionics* **1999**, *118*, 195.